

**The Philippine Earth Data Resource and Observation Center –  
An Enabler in Disaster Risk Reduction and Management**

Nash Frederic M. Prado<sup>1</sup>, Julius M. Judan<sup>1</sup>, Lianne Maxine A. Tabanggay<sup>1</sup>,  
Rocell Nino B. Vicente<sup>1</sup>, Harold Bryan S. Paler<sup>1</sup>, Alvin E. Retamar<sup>1</sup>

<sup>1</sup>DOST-Advanced Science and Technology Institute,  
ASTI Bldg., C.P. Garcia Ave, Quezon City, Philippines

Email: [nash@asti.dost.gov.ph](mailto:nash@asti.dost.gov.ph); [julius.judan@asti.dost.gov.ph](mailto:julius.judan@asti.dost.gov.ph); [lianne.tabanggay@asti.dost.gov.ph](mailto:lianne.tabanggay@asti.dost.gov.ph);  
[rocellvicente@asti.dost.gov.ph](mailto:rocellvicente@asti.dost.gov.ph); [harold@asti.dost.gov.ph](mailto:harold@asti.dost.gov.ph); [ning@asti.dost.gov.ph](mailto:ning@asti.dost.gov.ph)

**KEY WORDS:** Earth observation, Disaster risk

**ABSTRACT:** Satellite earth observation (EO) supports data-driven assessment and decision-making through the provision of timely information over a specific area of interest. This has become increasingly vital in the four thematic areas of disaster risk reduction and management – prevention and mitigation, preparedness, response and rehabilitation and recovery – as rapid assessments can be done for urgent and prompt action. Through the establishment of the Philippine Earth Data Resource and Observation (PEDRO) Center, the country now has improved access to very high resolution optical and synthetic aperture radar (SAR) imaging services, enabling the government to have on-demand coverage during critical events such as disasters, which shall be the primary application focus of this paper.

With the PEDRO Center’s ground receiving station, the project has reduced the latency in receiving satellite data, increasing its viability and reliability during events that require immediate action. It also has access to other satellite and complementary data resources. Received satellite images are subsequently processed, distributed to other government agencies and archived for further analyses or future use. Post-disaster images during typhoons and earthquakes have allowed first responders to better prioritize relief operations through rapid damage assessment. Likewise, flooding incidence have also been mapped through these data, allowing local governments to possibly integrate this with existing land use plans to reduce exposure. In the area of rehabilitation and recovery, satellite imaging has been essential in promoting transparency and accountability in validating the progress and extent of rebuilding damaged areas.

Although the provision of additional data has yielded positive results and outcomes, there is an inherent challenge in ensuring that these will be ingested and integrated in regular government workflows. Human resources of partner agencies must be trained to have the capacity to analyze and process spatial data to develop higher-order applications.

## 1. INTRODUCTION

With the cumulative impact of natural disasters, global warming and trends in population, the Philippines remains susceptible to disaster risk, exposing it to economic losses, crises, and mortality. From 2007 to 2016, the Philippines had already lost an equivalent of over 19.2 billion USD over 187 selected disasters (Agub and Turingan, 2017), making it one of the most vulnerable nations to disaster with a score of 25.14 in the WorldRiskIndex; the third highest worldwide (Bündnis Entwicklung Hilft, 2018).

A high-risk incidence requires a highly adaptive response mechanism to promote resilient communities. With recent development and easier access to earth observation (EO) satellites, many countries are now applying EO-derived information to aid in disaster risk reduction and management

(DRRM). EO, coupled with Geographic Information Systems (GIS) and Remote Sensing (RS), can be intensively utilized to generate rapid response, mapping, assessment and decision-making in times of disaster.

The use of GIS and RS, through data acquisition and emergency mapping, has long been employed and integrated in the DRRM efforts of the Philippines. However, it was not until 2016 that the Philippines, through the Department of Science and Technology (DOST) and the University of the Philippines (UP) launched its very own microsatellite Diwata-1 into space – which also signified the inception of the Philippine Earth Data Resource and Observation (PEDRO) Center.

The DOST-Advanced Science and Technology Institute (DOST-ASTI) is home to the PEDRO Center. The facility, with one located in Quezon City and the other in Davao City, enables the country to upload commands and download data from its supported satellites of different capacities. The available data are then archived, processed and distributed to applicable agencies and academic institutions for research, development and extension work related to disaster response, urban-change detection and environmental monitoring, among others.

The establishment of the PEDRO Center allowed for a more efficient utilization of national resources by significantly reducing single engagements with third-party satellite data providers. This also improved the government's response and provision of humanitarian relief, particularly during emergencies. The facility's readily available, direct reception of satellite data allows near real-time development and distribution of GIS products for the use of responsible entities in their subsequent site implementation, decision-making and policy formulation.

This paper aims to showcase the PEDRO Center and its applications in its attempt to adhere to the four thematic areas of DRRM: prevention and mitigation, preparedness, response and rehabilitation and recovery.

## **2. METHODS**

With direct access to very high and high-resolution imagery, the PEDRO Center applies various RS techniques and GIS analysis to provide usable information to partner government agencies. The commonly used methodologies for the team's operations are as follows:

### **2.1 Multicriteria evaluation for landslide hazard mapping**

Landslide hazard mapping often considers different factors in determining the susceptibility of a slope failing. These typically include slope angle, geology/lithology, elevation, peak ground acceleration (PGA), land cover, distance from roads, rivers, and fault lines (Chalkias et al., 2014; Akbari et al., 2014; Yan et al., 2013). These factors contribute to the instability of slopes regardless of triggering mechanism (earthquake or rainfall). However, research studies that combine these factors have variations in terms of weight or importance. Some studies would prioritize land cover (Chalkias et al., 2014), while other studies would consider slope angle as the highest contributing factor to the likelihood of a slope failing (Kayastha et al., 2013). Knowledge on the hierarchy of these factors are refined as more landslides occur and more studies are conducted based on new data. This is done using remote sensing (RS) and geographic information systems (GIS) techniques. In RS, immediate acquisition of satellite images after a landslide event is crucial because over time, vegetation would start covering the landslide scarp and thus, making it more difficult to recognize, map, and analyze in future satellite image acquisitions. GIS is then used to compile the different subfactors and weights are assigned based on historical landslide data over the site and other areas

with similar conditions (lithology, climate, etc.). Once the data is ready (subfactor maps prepared and weights assigned), a weighted overlay analysis is done by combining or stacking the different subfactor maps (Figure 1) to produce a landslide susceptibility map of the area.

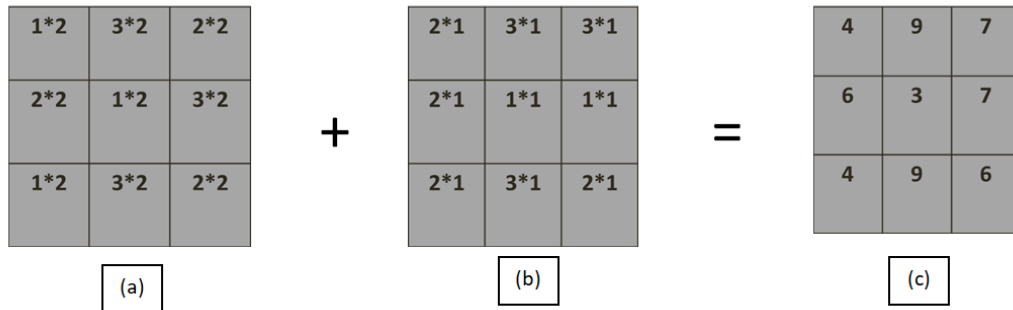


**Figure 1.** A schematic diagram of a weighted overlay analysis in a GIS platform.

The subfactors from each factor map (a & b) are assigned weights (1 to 5) wherein 1 means that it has the least amount of contribution to slope instability and 5 the highest. These subfactor weights are then multiplied to the weight value of the factor map (e.g., a = 2, b = 1). After assigning weights, all the factor maps' values whose areas geographically coincide with each other are added to produce the final map (c).

## 2.2 SAR intensity change detection for post-typhoon flood assessment

SAR satellites are ideal data sources for flood mapping because of its capability to provide its own illumination in the microwave range. As such, SAR satellites can be used for near all-weather night and day imaging situations and are independent of atmospheric conditions (Martinis and Rieke, 2015).

Figure 2 shows the workflow used in intensity change detection. After applying pre-processing and correction, amplitude-based intensity change computation can now be applied to both data sets. This measures the changes in total backscattering between the two SAR images, resulting to an intensity change map. A minimum threshold of 95% was applied to the intensity change map to extract areas that have highest percentage of changes, possibly alluding these changes to flooding.

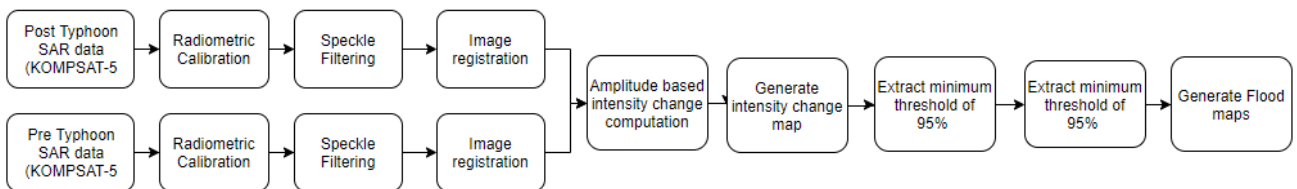


**Figure 2.** Workflow for extracting flood maps using intensity change map from pre- and post-typhoon images.

## 2.3 Normalized Burn Ratio for wildfire intensity

Burn severity is defined as the extent to which soil and vegetation had changed after fires (Parks, Dillon, and Miller, 2014). The Normalized Burn Ratio (NBR) was designed to identify possible burnt areas and estimate the severity of wildfires and volcanic eruptions. The NBR (1) shares the same

concept with the Normalized Difference Vegetation Index (NDVI), but instead of using the Near-Infrared (NIR) band, it utilizes the Short-Wave Infrared (SWIR) band as the damaged vegetation provides a higher reflectance on this portion of the spectrum (Suwarsono, Listi, Prasasti, and Khomarudin, 2018).

$$\text{Normalized Burn Ratio} = \frac{\text{NIR} - \text{SWIR}}{\text{NIR} + \text{SWIR}} \quad (1)$$

The values derived from the NBR could be categorized to further assess the severity of the damage, as seen in Table 1.

**Table 1.** Categorized value of change in normalized burn ratio (FIREMON, 2004).

$\Delta\text{NBR}$	Burn Severity
< - 0.25	High post-fire regrowth
-0.25 to -0.1	Low post-fire regrowth
-0.1 to 0.1	Unburned
0.1 to 0.27	Low-severity burn
0.27 to 0.44	Moderate-low severity burn
0.44 to 0.66	Moderate-high severity burn
> 0.66	High-severity burn

### 3. RESULTS AND DISCUSSIONS

#### 3.1 Multicriteria evaluation of the Magnitude 6.5 Leyte Earthquake

In this scenario, two aspects of PEDRO's contribution to disaster risk reduction is highlighted. A short-term solution for disaster response and a long-term contribution to studies that need landslide inventory data for susceptibility modelling and mapping.

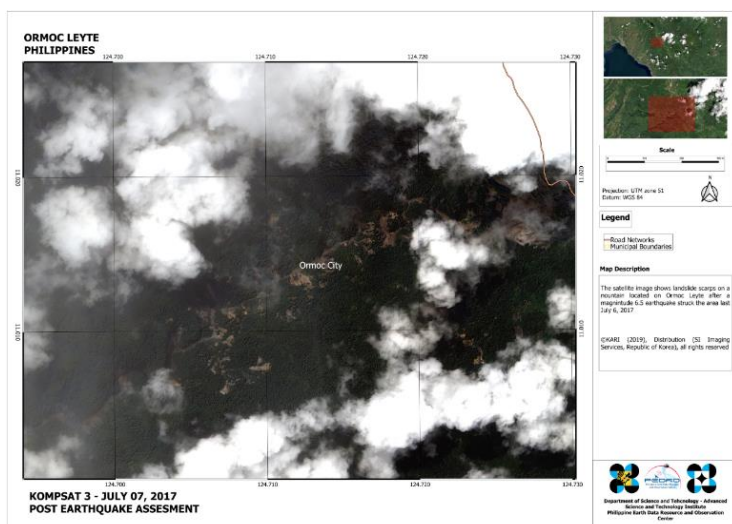


**Figure 3.** Landslide scarps caused by the M6.5 Leyte earthquake. Includes material ©KARI 2017, Distribution (SI Imaging Services, Republic of Korea), all rights reserved.

On July 6, 2017, a magnitude 6.5 earthquake struck Leyte with the epicenter originating 6.5 km north-northeast of Ormoc City (Yang et al., 2018). Once reports were confirmed, the PEDRO Center immediately tasked all available satellites to acquire an image over the area. A Komsat-3 image was downloaded on July 10, 2017 (Figure 3) and shared with the relevant agency: the Philippine Institute of Volcanology and Seismology (PHIVOLCS).

Despite the abundance of cloud cover, landslide scarps are visible in the image (Figure 3). These were confirmed to have been caused by the earthquake based on archive images (the scarps were not present in a June 29, 2017 Landsat image of the same area). It only took a few days to acquire an image despite the cloud cover, highlighting the value of having a ground station in times of disaster.

The mapped landslide scarps were also useful for long-term research. Different thematic maps were prepared and formatted to be used in a GIS platform to evaluate what conditions were present on the areas where the landslides occurred (Figure 4, left-to-right): (1) geologic map [digitized from a lithologic map from the Mines and Geosciences Bureau {MGB}]; (2) slope map [derived from a Digital Elevation Model {DEM} from the Phil-Lidar program]; (3) land cover map [from the National Mapping and Resource Information Authority {NAMRIA}]; (4) distance from fault map [processed and digitized from a fault map of PHIVOLCS]; (5) distance from rivers map [digitized from a topographic map of NAMRIA]; and (6) distance from roads map [digitized from a topographic map from NAMRIA].

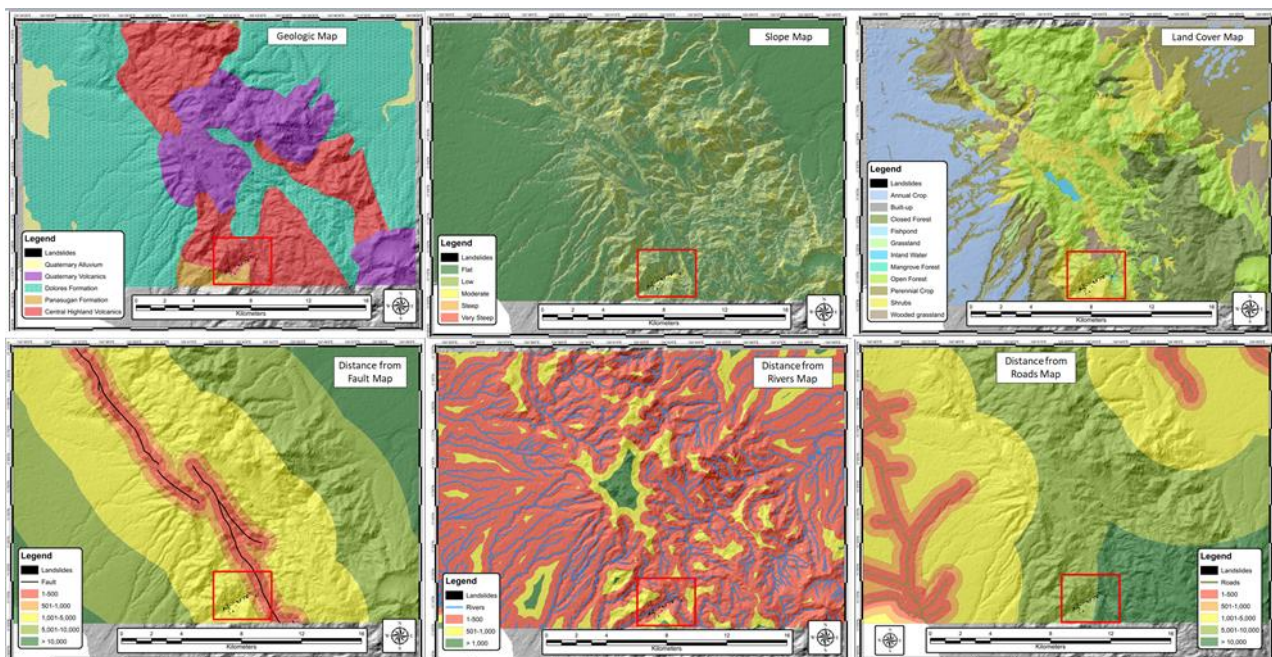


**Figure 4.** Six (6) subfactor/thematic maps were prepared and correlated with the mapped landslide scarps to determine what influences slope failure and to better predict when and where future landslides might occur.

Based on the correlation of the landslide scarps and the different maps, the categories with the highest influence on the occurrence of the landslides are geology and the proximity to rivers. As more landslides occur and more satellite images are acquired, more data can be used to fine-tune the rankings of the different subfactors that may influence landslide occurrence, thus, producing more reliable landslide hazard maps, and hopefully, lessening the number of casualties and affected communities.

### 3.2 Rapid response for post-typhoon flood assessment using SAR

On July 16, 2019, Tropical Storm Danas made landfall in the northern provinces of the Philippines, affecting around 758 families across the region (NDRRMC, 2019). National roads and seaports across the area were closed due to soil erosion and flooding, respectively. Due to the lack of on-site accessibility, the PEDRO Center had tasked SAR satellite KOMPSAT-5 to capture images over the areas of Aparri, Cagayan on July 16, 2019.

Figure 5 features the use of the KOMPSAT-5 images for pre- and post-typhoon flood assessment using intensity change detection.

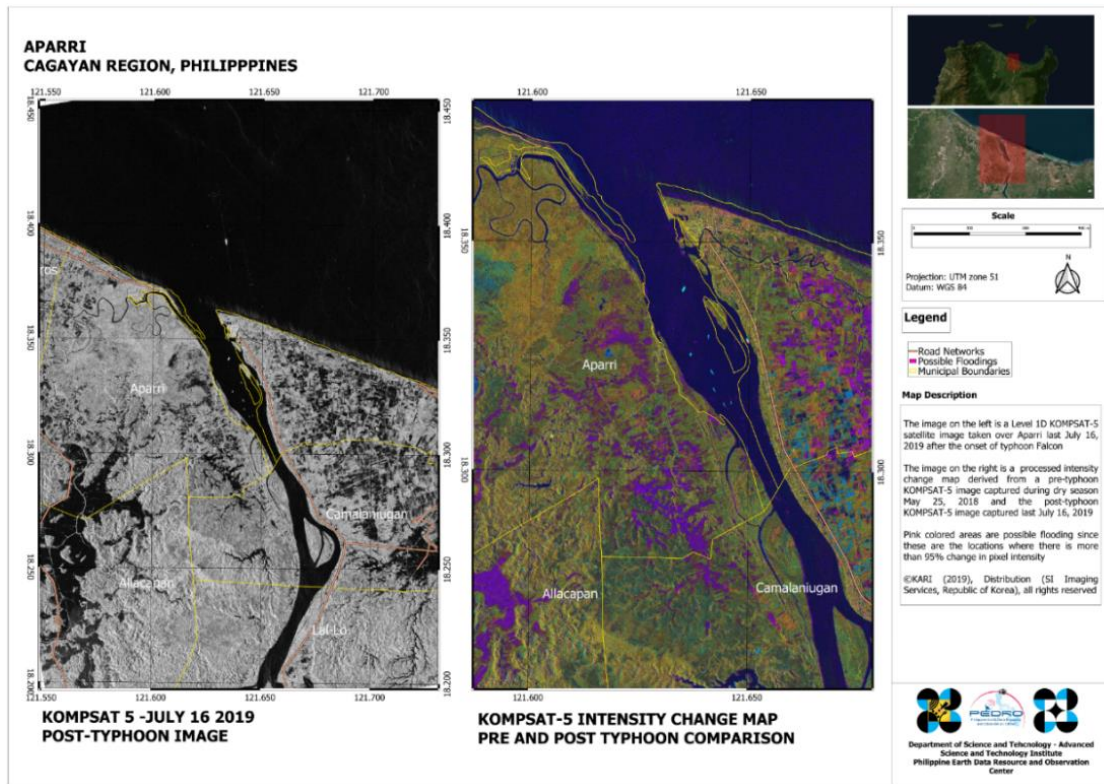


**Figure 5.** A KOMPASAT-5 satellite image showing the areas affected by Tropical Storm Danas. Includes material ©KARI 2019, Distribution (SI Imaging Services, Republic of Korea), all rights reserved.

The image on the right pane has reflected flooding due to an increase in pixel intensity (95%), as shown by the violet-shaded areas. Using change detection, the PEDRO Center was able to extract flood maps for the region in support of response and rehabilitation activities of mandated local units. Moreover, these flood maps can be used to update land use plans for a long-term mitigation strategy.

### 3.3 Determining wildfire severity from the Mt. Apo wildfire

On 26 March 2016, the country's highest mountain, Mt. Apo, recorded a wildfire incident which ravaged the mountain's summit. Using satellite images with the disciplines of RS and GIS, the PEDRO Center was able to document this incident.

An estimated area of 110 hectares was burned by the wildfire last April 2, 2016 based on the satellite images provided by Sentinel-2A (Figure 6).

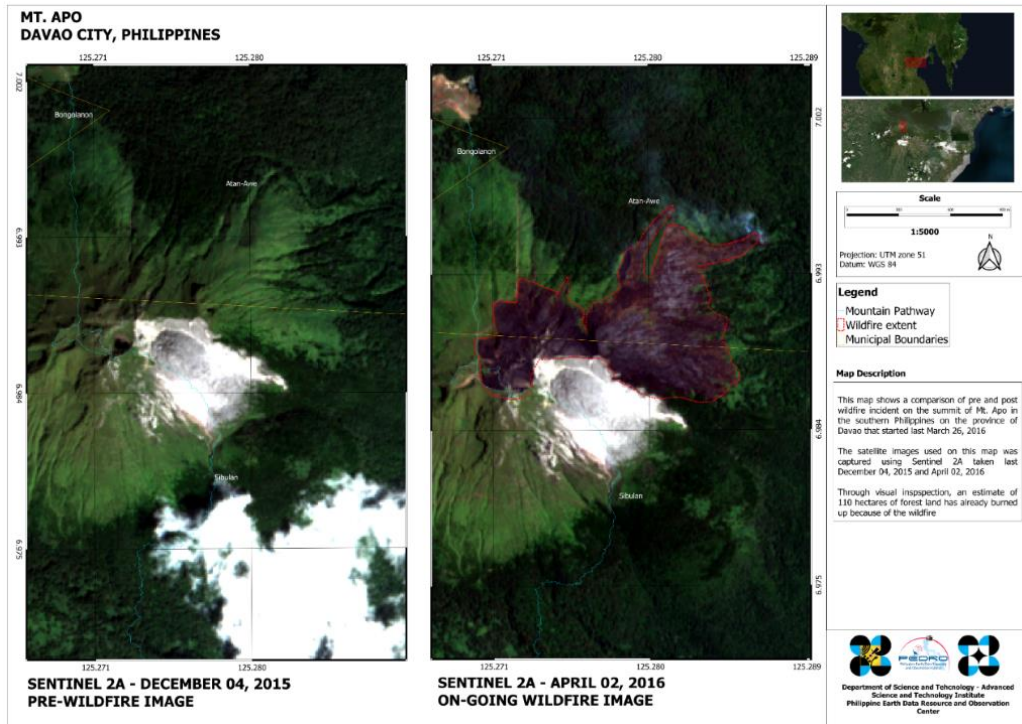


**Figure 6.** Open-source Sentinel-2A satellite images captured before and after the wildfire. Includes Copernicus Sentinel data [2015, 2016].

The  $\Delta NBR$  was computed from the NBR of a pre-fire image (dated December 04, 2015) and a post-fire image (dated April 02, 2016), as seen in Figure 7. Darker red areas highlight higher burn severity.

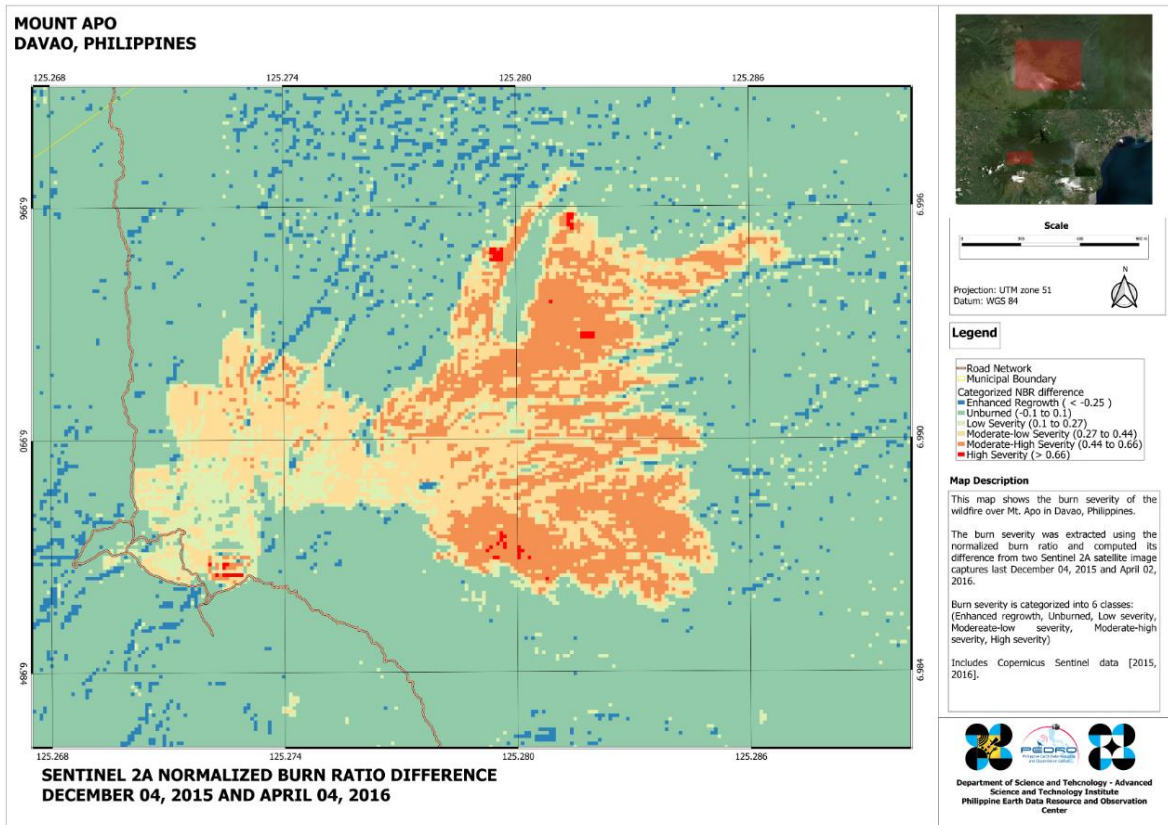


**Figure 7.**  $\Delta$ NBR map showing the wildfire severity at Mt. Apo, Davao City, Philippines. *Includes Copernicus Sentinel data [2015, 2016].*

Through the assessment of the NBR, disaster management agencies can better focus their response efforts to the most severely hit areas, allowing for a more efficient deployment and mobilization of government resources.



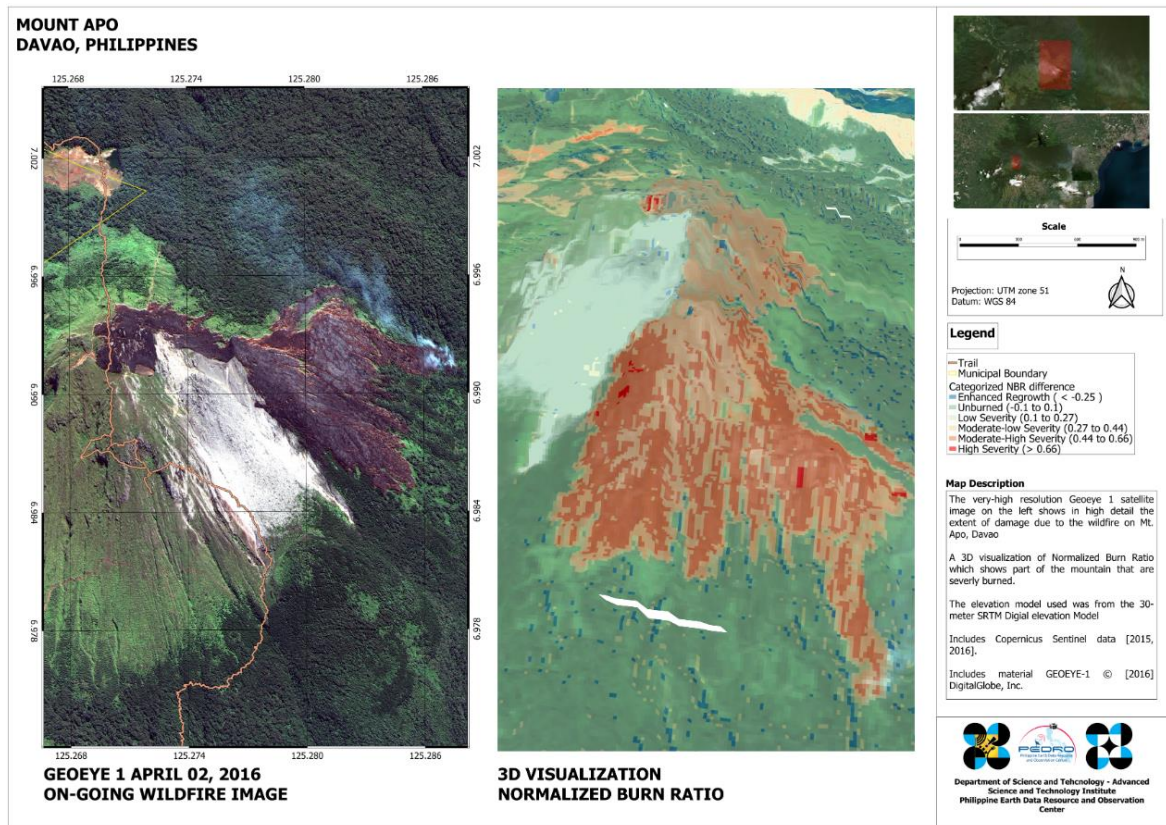


**Figure 8.** Quantitative damage assessment through visual inspection of the extent of the wildfire in Mt. Apo in Davao City, Philippines. *Includes material GEOEYE-1 © [2016] DigitalGlobe, Inc.*

#### 4. CONCLUSION

The scenarios and cases highlighted in this paper detail the possible contributions of RS and GIS in DRRM. The direct availability of EO data creates high-quality supplemental information to better implement disaster-linked efforts in the Philippines.

Flood maps can form part of a city’s pre-disaster risk assessment, allowing them to better administer their resources in preparation of an upcoming hydrometeorological disaster. On-demand maps on the severity of landslides, earthquakes or wildfire can lead to better planning and mobilization of government resources as a response to these critical events. Moreover, EO data can also keep track of rehabilitation efforts after disasters, promoting accountability and transparency.

Moving forward, further capacity-building activities must be performed to give government agencies the capability to process and analyze EO data in-house. This will further integrate the use of RS and GIS in their regular operational workflows, improving overall efficiency in the delivery of public services.

## 5. REFERENCES

- Agub, Sherwynne B. and Turingan, Peter Anthony S. 2017. *Senate Economic Planning Office Policy Brief*. 17 (1). Pasay City, Manila, Philippines. Retrieved from: [https://www.senate.gov.ph/publications/SEPO/PB\\_Examining%20PH%20DRRM%20System\\_Revised\\_27June2017.pdf](https://www.senate.gov.ph/publications/SEPO/PB_Examining%20PH%20DRRM%20System_Revised_27June2017.pdf)
- Akbari, Abolghasem, Bin Mat Yahaya, Fadzil, Azamirad, Mahmoud, and Fanodi, Mohsen. 2014. *Landslide susceptibility mapping using logistic regression analysis and GIS tools*. EJGE Vol. 19 [2014].
- Bündnis Entwicklung Hilft. 2018. *WorldRiskReport 2018*. Germany. Obtained from: [https://weltrisikobericht.de/wp-content/uploads/2019/03/190318\\_WRR\\_2018\\_EN\\_RZonline\\_1.pdf](https://weltrisikobericht.de/wp-content/uploads/2019/03/190318_WRR_2018_EN_RZonline_1.pdf)
- Chalkias, Christos, Ferentinou, Maria, and Polykretis, Christos. 2014. *GIS-based landslide susceptibility mapping on the Peloponnese Peninsula, Greece*. Geosciences 2014, 4, 176-190; doi:10.3390/geosciences4030176.
- Fire Research and Management Exchange System (FIREMON). 2004. *FIREMON BR cheat sheet V4*. Retrieved from: [http://burnseverity.cr.usgs.gov/pdfs/LAv4\\_BR\\_CheatSheet.pdf](http://burnseverity.cr.usgs.gov/pdfs/LAv4_BR_CheatSheet.pdf)
- Kayastha, P., Dhital, M.R., De Smedt, F.. 2013. *Application of the analytical hierarchy process (AHP) for landslide susceptibility mapping: A case study from the Tinau watershed, west Nepal*. P. Kayastha et al. / Computers & Geosciences 52 (2013) 398–408.
- Martinis, Sandro & Rieke, Christoph, 2015. *Backscatter analysis using Multi-temporal and Multi-frequency SAR Data in the context of flood mapping*. Remote Sens. 2015 7, 7732-7752; doi:10.3390/rs70607732.
- National Disaster Risk Reduction and Management Council (NDRRMC). 2019. *Sitrep No. 04 re Preparedness Measures for Tropical Depression "FALCON"*. Retrieved from: [http://www.ndrrmc.gov.ph/attachments/article/3830/Update\\_Sitrep\\_no\\_4\\_re\\_Preparedness\\_Measures\\_and\\_Effects\\_of\\_Tropical\\_Storm\\_FALCON\\_as\\_of\\_6PM\\_issued\\_on\\_17\\_July\\_2019.pdf](http://www.ndrrmc.gov.ph/attachments/article/3830/Update_Sitrep_no_4_re_Preparedness_Measures_and_Effects_of_Tropical_Storm_FALCON_as_of_6PM_issued_on_17_July_2019.pdf)
- Parks, Sean A., Dillon, Gregory K., and Miller, Carol. 2014. *A New Metric for Quantifying Burn Severity: The Relativized Burn Ratio*. Remote Sens. 2014 6, 1827-1844; doi:10.3390/rs6031827
- Suwarsono, Hana, Listi, Hana, Prasasti, Indah, and Khomarudin, Rokhis. 2018. *Mapping burned areas from landsat-8 imageries on mountainous region using reflectance changes*. MATEC Web of Conferences. 229. 04012. 10.1051/mateconf/201822904012.
- Yan, Bao, Zhi-Jian, Huang, Yun-Jie, Wei, Lian-Jin, Tao, and Hong-Hu, Wei. 2013. *Landslide hazard assessment based on fuzzy synthesis judgment and geographic information system*. Appl. Math. Inf. Sci. 7, No. 3, 1125-1128 (2013)
- Yang, Y.H., Tsai, M.C., Hu, J.C., Aurelio, M. A., Hashimoto, M., Escudero, J. A. P., Chen, Q. 2018. *Coseismic slip deficit of the 2017 Mw 6.5 Ormoc earthquake that occurred along a creeping segment and geothermal field of the Philippine fault*. Geophysical Research Letters, 45(6), 2659–2668. doi:10.1002/2017gl076417.